JSR Publications

Available Online

J. Sci. Res. **4** (2), 337-348 (2012)

JOURNAL OF SCIENTIFIC RESEARCH

www.banglajol.info/index.php/JSR

Effects of Reynolds and Prandtl Number on Mixed Convection in an Octagonal Channel with a Heat-Generating Hollow Cylinder

S. Parvin[*] and R. Nasrin

Department of Mathematics, Bangladesh University of Engineering and Technology, Dhaka-1000, Bangladesh

Received 2 August 2011, accepted in final revised form 31 December 2011

Abstract

A numerical study has been executed to analyze the effects of Reynolds and Prandtl number on mixed convective flow and heat transfer characteristics inside an octagonal vertical channel in presence of a heat-generating hollow circular cylinder placed at the centre. All the walls of the octagon are considered to be adiabatic. Galerkin weighted residual finite element method is used to solve the governing equations of mass, momentum and energy. Results are presented in terms of streamlines, isotherms, the average Nusselt number and the maximum fluid temperature for different combinations of controlling parameters namely, Reynolds number, Prandtl number and Richardson number. The results indicate that the flow and thermal fields as well as the heat transfer rate and the maximum fluid temperature in the octagonal channel depend significantly on the mentioned parameters.

Keywords: Heat-generation; Hollow cylinder; Octagonal channel; Mixed convection; Finite element method.

doi: http://dx.doi.org/10.3329/jsr.v4i2.8142 J. Sci. Res. **4** (2), 337-348 (2012)

1. Introduction

Because of its practical importance, mixed convection in channels is of great interest of the phenomenon in many technological processes, such as the design of solar collectors, thermal design of buildings, air conditioning and the cooling of electronic circuit boards. In recent years, modification of heat transfer in channels due to introduction of obstacles, partitions and fins attached to the wall(s) has received sustained attention. A literature review on the subject shows that many authors have considered mixed convection in vented enclosures with obstacles, partitions and fins, thereby altering the convection flow phenomenon.

Actual enclosures in practice are often found to have different shapes rather than rectangular ones. Some examples of non-rectangular channels include various channels of constructions, panels of electronic equipment and solar energy collectors etc. Several

[*] *Corresponding author*: salpar@math.buet.ac.bd

geometrical configurations, more or less complex, have been examined under theoretical, numerical or experimental approaches.

Calmidi and Mahajan [1] studied mixed convection in a partially divided rectangular enclosure over a wide range of Reynolds and Grashof numbers. Their findings were that the average Nusselt number and the dimensionless surface temperature depended on the location and height of the divider. Omri and Nasrallah [2] conducted mixed convection in an air-cooled cavity with differentially heated vertical isothermal sidewalls having inlet and exit ports by a control volume finite element method. They investigated two different placement configurations of the inlet and exit ports on the sidewalls. Best configuration was selected analyzing the cooling effectiveness of the cavity, which suggested that injecting air through the cold wall was more effective in heat removal and placing inlet near the bottom and exit near the top produced effective cooling. Later on, Singh and Sharif [3] extended their works by considering six placement configurations of the inlet and exit ports of a differentially heated rectangular enclosure whereas the previous work was limited only two different configurations of inlet and exit port. At the same time, a numerical analysis of laminar mixed convection in an open cavity with a heated wall bounded by a horizontally insulated plate was presented by Manca *et al*. [4], where three heating modes were considered: assisting flow, opposing flow and heating from below. Results were reported for Richardson number from 0.1 to 100, Reynolds numbers from 100 to 1000 and aspect ratio in the range 0.1–1.5. They showed that the maximum temperature values decreased as the Reynolds and the Richardson numbers increased. The effect of the ratio of channel height to the cavity height was found to play a significant role on streamline and isotherm patterns for different heating configurations. The investigation also indicated that opposing forced flow configuration had the highest thermal performance, in terms of both maximum temperature and average Nusselt number. Later, similar problem for the case of assisting forced flow configuration was tested experimentally by Manca *et al*. [5] and based on the flow visualization results, they pointed out that for Re = 1000 there were two nearly distinct fluid motions: a parallel forced flow in the channel and a recirculation flow inside the cavity and for Re = 100, the effect of a stronger buoyancy determined a penetration of thermal plume from the heated plate wall into the upper channel. Numerical study on mixed convection in a square cavity due to heat generating rectangular body was carried out by Shuja *et al*. [6]. They investigated the effect of exit port locations on the heat transfer characteristics and irreversibility generation in the cavity and showed that the normalized irreversibility increased as the exit port location number increased and the heat transfer from the solid body enhanced while the irreversibility reduced. Hung and Fu [7] studied the passive enhancement of mixed convection heat transfer in a horizontal channel with inner rectangular blocks by geometric modification. Unsteady mixed convection in a horizontal channel containing heated blocks on its lower wall was studied numerically by Najam *et al*. [8]. Tsay *et al*. [9] rigorously investigated the thermal and hydrodynamic interactions among the surface-mounted heated blocks and baffles in a duct flow mixed convection. They focused particularly on the effects of the height of baffle, distance between the

heated blocks, baffle and number of baffles on the flow structure and heat transfer characteristics for the system at various *Re* and Gr/Re^2. Bhoite *et al*. [10] studied numerically the problem of mixed convection flow and heat transfer in a shallow enclosure with a series of block-like heat generating component for a range of Reynolds and Grashof numbers and block-to-fluid thermal conductivity ratios. They showed that higher Reynolds number tend to create a recirculation region of increasing strength at the core region and the effect of buoyancy becomes insignificant beyond a Reynolds number of typically 600, and the thermal conductivity ratio had a negligible effect on the velocity fields. Brown and Lai [11] numerically studied a horizontal channel with an open cavity and obtained correlations for combined heat and mass transfer which covered the entire convection regime from natural, mixed to forced convection. Rahman *et al*. [12] studied numerically the opposing mixed convection in a vented enclosure. They found that with the increase of Reynolds and Richardson numbers the convective heat transfer became predominant over the conduction heat transfer and the rate of heat transfer from the heated wall was significantly depended on the position of the inlet port. Saha *et al*. [13] performed natural convection heat transfer within octagonal enclosure. Their results showed that the effect of *Ra* on the convection heat transfer phenomenon inside the enclosure was significant for all values of *Pr* studied (0.71-50). It was also found that, *Pr* influence natural convection inside the enclosure at high *Ra* ($Ra > 10^4$). Rahman *et al*. [14] developed the magnetic field effect on mixed convective flow in a horizontal channel with a bottom heated open enclosure. Their results indicated that the magnetic field strongly affected the flow phenomenon and temperature field inside the cavity whereas this effect was less significant in the channel. Very recently, Nasrin [15] performed aspect ratio effect of vertical lid driven chamber having a centered conducting solid on mixed magnetoconvection. The author showed that maximum rate of heat transfer is observed for the lowest aspect ratio *AR* owing to the shortest distance between the hot and cold surfaces. Also, Joule heating effect on MHD combined convection in a wavy chamber having conducting square cylinder was studied by Nasrin [16].

On the basis of the literature review, it appears that no work was reported on mixed convection in an octagonal channel with heat generating circular block. The present study addresses the effects of Reynolds number, Prandtl number and Richardson number on the thermal and flow fields for such geometry. The numerical computation covers a wide range of Reynolds number ($5 \le Re \le 50$), Prandtl number ($0.73 \le Pr \le 7$) and Richardson number ($0 \le Ri \le 10$).

2. Model Specification

The geometry of the problem herein investigated is depicted in Fig. 1. The system consists of an octagonal channel with sides of length *L*, within which a heat generating hollow circular body with outer diameter *d* is centered. The hollow circular body has a thermal conductivity of k_s and generates uniform heat *q* per unit volume. All solid walls of the octagon are considered to be adiabatic. It is assumed that the incoming flow has a uniform

velocity, v_i and temperature, T_i. The inlet opening is located at the bottom, whereas the outlet opening is at the top of the octagon.

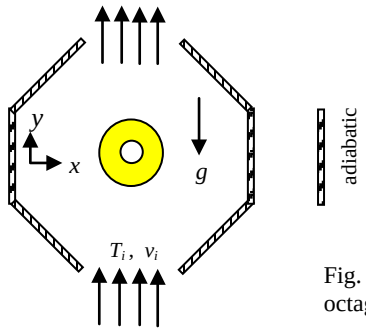

Fig. 1. Physical model of the octagonal channel.

3. Mathematical Formulation

A two-dimensional, steady, laminar, incompressible, mixed convection flow is considered within the channel and the fluid properties are assumed to be constant. The radiation effects are taken as negligible. The dimensionless equations describing the flow under Boussinesq approximation are as follows [10, 11]:

$$\frac{\partial U}{\partial X}+\frac{\partial V}{\partial Y}=0 \tag{1}$$

$$U\frac{\partial U}{\partial X}+V\frac{\partial U}{\partial Y}=-\frac{\partial P}{\partial X}+\frac{1}{Re}\left(\frac{\partial^2 U}{\partial X^2}+\frac{\partial^2 U}{\partial Y^2}\right) \tag{2}$$

$$U\frac{\partial V}{\partial X}+V\frac{\partial V}{\partial Y}=-\frac{\partial P}{\partial Y}+\frac{1}{Re}\left(\frac{\partial^2 V}{\partial X^2}+\frac{\partial^2 V}{\partial Y^2}\right)+Ri\,\theta \tag{3}$$

$$U\frac{\partial \theta}{\partial X}+V\frac{\partial \theta}{\partial Y}=\frac{1}{RePr}\left(\frac{\partial^2 \theta}{\partial X^2}+\frac{\partial^2 \theta}{\partial Y^2}\right) \tag{4}$$

For solid cylinder the energy equation is

$$\frac{\partial^2 \theta_s}{\partial X^2}+\frac{\partial^2 \theta_s}{\partial Y^2}+Q=0 \tag{5}$$

where $Re=\frac{v_i L}{\nu}$, $Pr=\frac{\nu}{\alpha}$ and $Ri=\frac{g\beta\Delta TL}{v_i^{\,2}}$ are Reynolds number, Prandtl number and Richardson number respectively and $Q=\frac{qL^2}{k_s\Delta T}$ is the heat generating parameter.

The above equations are non-dimensionalized by using the following dimensionless quantities

$$X=\frac{x}{L},\ Y=\frac{y}{L},\ D=\frac{d}{L},\ U=\frac{u}{v_i},\ V=\frac{v}{v_i},\ P=\frac{p}{\rho v_i^{\,2}},\ \theta=\frac{(T-T_i)}{(T_h-T_i)},\ \theta_s=\frac{(T_s-T_i)}{(T_h-T_i)}$$

where X and Y are the coordinates varying along horizontal and vertical directions respectively, U and V are the velocity components in the X and Y directions respectively, θ is the dimensionless temperature and P is the dimensionless pressure.

The boundary conditions for the present problem are specified as follows:

at the inlet: $U = 0$, $V = 1$, $\theta = 0$

at the outlet: convective boundary condition $P = 0$

at all solid boundaries: $U = 0, V = 0$

at the walls of the octagon: $\dfrac{\partial \theta}{\partial N} = 0$

at the fluid-solid interface: $\left(\dfrac{\partial \theta}{\partial N}\right)_{fluid} = K\left(\dfrac{\partial \theta_s}{\partial N}\right)_{solid}$

where N is the non-dimensional distances either X or Y direction acting normal to the surface and K is the dimensionless ratio of the thermal conductivity $\left(k_s / k_f\right)$.

The average Nusselt number at the heat generating body may be expressed as

$$Nu = -\frac{1}{L_s}\int_0^{L_s} \frac{\partial \theta}{\partial n}\, dS$$

where $\dfrac{\partial \theta}{\partial n} = \sqrt{\left(\dfrac{\partial \theta}{\partial X}\right)^2 + \left(\dfrac{\partial \theta}{\partial Y}\right)^2}$, L_s and S are the length and coordinate along the circular surface respectively.

4. Computational Procedure

The Galerkin finite element method [17, 18] is used to solve the non-dimensional governing equations along with boundary conditions for the considered problem. The equation of continuity has been used as a constraint due to mass conservation and this restriction may be used to find the pressure distribution. The penalty finite element method [19] is used to solve the Eqs. (2) to (4), where the pressure P is eliminated by a penalty constraint. The continuity equation is automatically fulfilled for large values of this penalty constraint. Then the velocity components (U, V), and temperature (θ) are expanded using a basis set. The Galerkin finite element technique yields the subsequent nonlinear residual equations. Three points Gaussian quadrature is used to evaluate the integrals in these equations. The non-linear residual equations are solved using Newton-Raphson method to determine the coefficients of the expansions. The convergence of solutions is assumed when the relative error for each variable between consecutive iterations is recorded below the convergence criterion ε such that $\left|\psi^{n+1} - \psi^{n}\right| \le 10^{-4}$, where n is the number of iteration and Ψ is a function of U, V, and θ.

4.1. *Grid refinement check*

In order to determine the proper grid size for this study, a grid independence test is conducted with five types of mesh for Pr = 1.73, Re = 50, Ri = 1, Q = 5, K = 5 and D = 0.3. The extreme values of Nu and θ_{max} are used as a sensitivity measure of the accuracy of the solution and are selected as the monitoring variables. Considering both the accuracy

of numerical values and computational time, the present calculations are performed with 40295 nodes and 10936 elements grid system.

Table 1. Grid sensitivity check at Pr = 1.73, Re = 50, Ri = 1, Q = 5, K = 5 and D = 0.3.

Nodes (elements)	7224 (4816)	12982 (5784)	26538 (8992)	40295 (10936)	80524 (18080)
Nu	5.312753	5.526821	5.615743	5.716742	5.716743
θ_{max}	1.132832	1.091826	1.079835	1.051825	1.051824
Time (s)	226.265	292.594	388.157	421.328	627.375

5. Results and Discussion

The mixed convection phenomenon inside a two sided open octagon having a heat-generating hollow circular block is influenced by different controlling parameters such as Reynolds number Re, Richardson number Ri, Prandtl number Pr, solid fluid thermal conductivity ratio K, heat generating parameter Q and diameter D of the circular body. Analysis of the results is made through obtained streamlines, isotherms, average Nusselt number and maximum temperature of the fluid for three significant parameters, Re, Pr and Ri. The ranges are varied as $5 \leq Re \leq 50$, $0.73 \leq Pr \leq 7$ and $0 \leq Ri \leq 10$, while the other parameters K, D and Q are kept fixed at 5, 0.3 and 5, respectively.

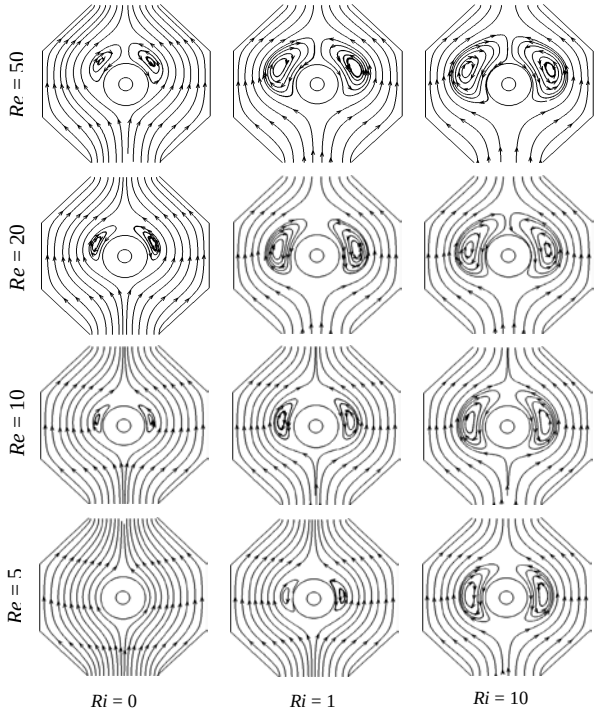

Fig. 2. Streamlines for various Re and Ri with Pr = 1.73, K = 5, D = 0.3 and Q = 5.

The effects of *Re* and *Ri* on streamlines and isotherms are shown in Figs. 2 and 3 for *Pr* = 1.73. For a fixed *Ri*, change of Reynolds number causes the change of Grashof number. In this study, the considered values of *Re* and *Ri* have not significant effect on Grashof number. The flow structure in the absence of the free convection effect (*Ri* = 0) is presented in the left column of the Fig. 2. For *Ri* = 0 and *Re* = 5 the fluid flow occupies almost the whole domain and bifurcates near the circular body. At this stage, the streamlines become symmetrical about the vertical line passing through the centre of the cylinder. It is seen that a pair of small vortices are developed adjacent to the heat generating cylinder at *Re* = 10, due to increased inertia force. Further more, the size of the vortex increases at *Re*= 20 for the fixed *Ri* (= 0). As the Reynolds number increases up to 50, the role of forced convection in the octagon is more significant and consequently the circulation cells in the flow become large. On the other hand, at any particular Reynolds number, a significant change in flow pattern is marked as the flow regime changes from dominant forced convection to dominant free convection with the increasing *Ri.*

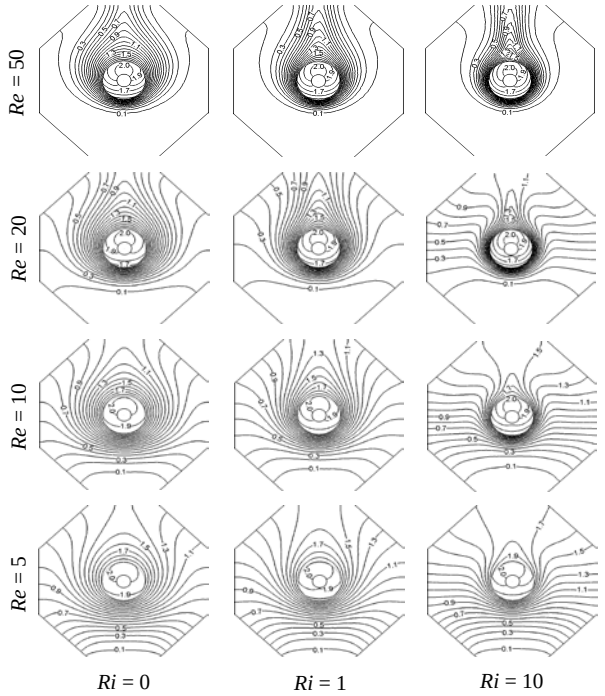

Fig. 3. Isotherms for various *Re* and *Ri* with *Pr* = 1.73, *K* =5, *D* = 0.3 and *Q* = 5.

The corresponding isotherm plots are presented in Fig. 3. From the figure, it is clear that Reynolds number has significant effect on isotherms at various convection regimes. It is observed that increase in *Re* reduces the thermal boundary layer thickness near the lower part of the heated body and consequently the isothermal lines disappear from the

bottom portion of the channel. This is because at larger value of *Re*, the effect of buoyancy force become negligible and the flow is governed by the forced convection. With increasing *Ri*, isotherms become denser and a thermal plume is formed based on the cylinder to the outlet at a particular *Re*.

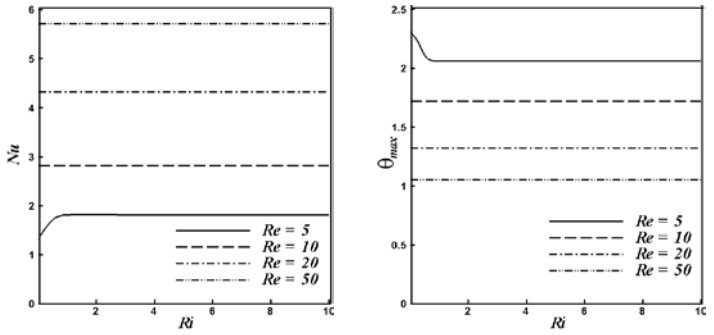

Fig. 4. Effect of Reynolds number on (i) average Nusselt number and (*left panel*) (ii) maximum temperature of fluid while *Pr* = 1.73 (*right panel*).

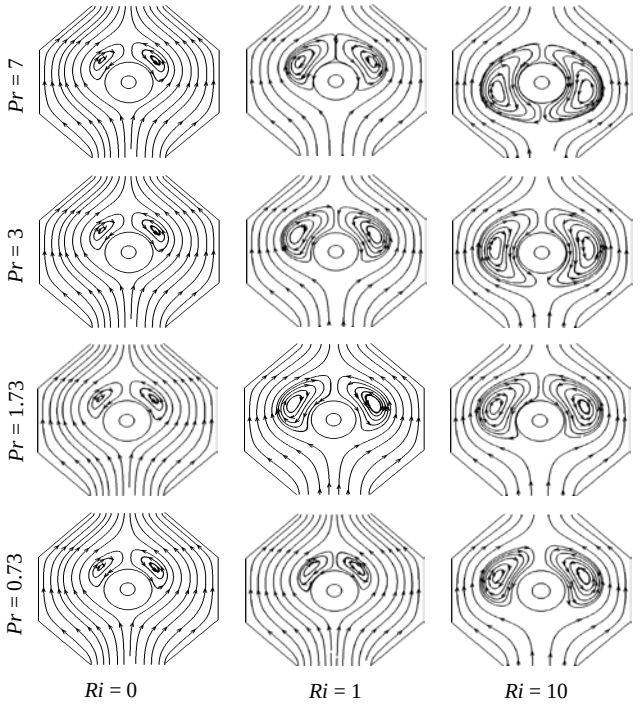

Fig. 5**.** Streamlines for various *Pr* and *Ri* with *Re* = 50, *K* =5, *D* = 0.3 and *Q* = 5.

Fig. 4 describes the effects of the Reynolds number *Re* on the average Nusselt number and maximum temperature of fluid along with *Ri*. It is noteworthy that the values of *Nu* remain stable with increasing *Ri* for upper values of *Re* (= 10, 20 and 50). But at *Re* = 5, it increases rapidly in the forced convection dominated region and becomes constant in the remaining region. The greatest heat transfer rate is found for the highest value of *Re*. This happens due to the heat transfer mechanism is affected by the strong external flow. On the other hand, the maximum temperature θ_{max} of the fluid decreases with rising *Re* while it is stabilized at higher values of *Re* due to the variation in *Ri*. At the lowest *Re*, it decreases sharply upto *Ri* = 1 and beyond this region, there is no variation in θ_{max}.

Figs. 5 - 6 provide the information about the influence of *Pr* at the three different values of *Ri* on streamlines as well as isotherms for *Re* = 50. The considered values of Prandtl number (*Pr*) mean air for the lowest value (*Pr* = 0.73) and the rest of the values (*Pr* = 1.73, 3 and 7) are for water in different temperatures. The flow with small Prandtl number at *Ri* = 0 creates a couple of tiny recirculation regions near the heat generating hollow cylinder as shown in Fig. 5. These recirculation regions remain almost identical for the four cases presented at *Ri* =0. The flow structure is not affected by varying *Pr* at the purely forced convection region, whereas it has noticeable change in other convection regimes. For a particular *Pr*, size of spinning cells becomes larger due to buoyancy force with increasing *Ri*.

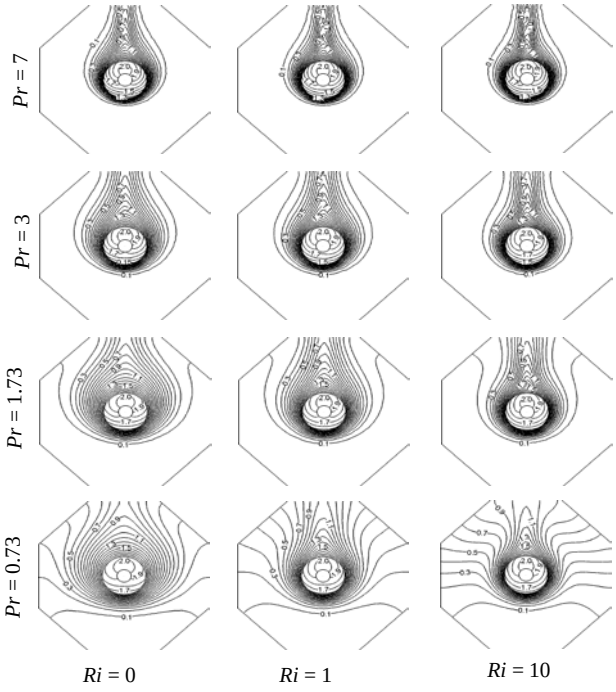

Fig. 6**.** Isotherms for various *Pr* and *Ri* with *Re* = 50, *K* =5, *D* = 0.3 and *Q* = 5.

The temperature field depending on *Pr* and *Ri* is illustrated in Fig. 6. Thermal boundary layer thickness reduces as *Pr* increases and the isothermal lines become denser at the adjacent area of the heat source. Also, for higher Prandtl number the isothermal lines disappear from the bottom part of the octagon and take an onion shape from the circular body to exit port. This is due to confining the thermal boundary layer in a small region for highly viscous fluid. The lines become more concentrated from the forced convection dominant region to free convection dominant region for a particular *Pr*.

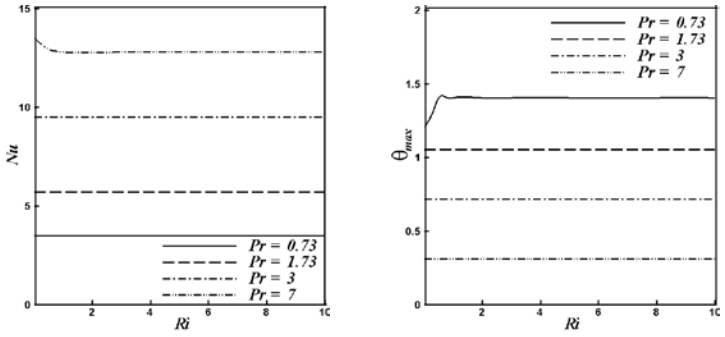

Fig. 7. Effect of Prandtl number *Pr* on (i) average Nusselt number (*left panel*) and (ii) maximum temperature of the fluid, while *Re* = 50 (*right panel*).

The variation of the average Nusselt number (*Nu*) at the heated surface and the maximum temperature of the fluid (θ_{max}) for different Prandtl numbers with Richardson numbers has been presented in Fig. 7. It is clearly seen from the figure that for a particular value of *Ri*, the average Nusselt number is the highest and maximum temperature of fluid is the lowest for the largest Prandtl number *Pr* = 7. This is because, the fluid with the highest Prandtl number is capable to carry more heat away from the heat source and dissipated through the out flow opening. On the other hand, *Nu* remains almost constant for lower values of Prandtl number. It decreases slightly for the highest *Pr* in the forced convection dominated region ($Ri \leq 1$) and beyond this region, it becomes flatten. Moreover, for the lowest value of *Pr*, θ_{max} grows up sharply upto *Ri* = 1 and then it is invariant with rising *Ri*. In addition, for the remaining *Pr*, it is constant with varying *Ri*.

6. Conclusion

A computational study is performed to investigate the mixed convection in an octagonal channel with a heat-generating horizontal circular body. Results are obtained for wide ranges of Reynolds number *Re*, Richardson number *Ri* and Prandtl number *Pr*. The following conclusions may be drawn from the present investigations:

- The forced convection parameter *Re* has a significant effect on the flow and temperature fields. Vortices created by inertia force in the streamlines increase and

thermal layer near the heated surface become thin and concentrated with increasing values of *Re*. Average Nusselt number at the heated surface increases as *Re* increases. The maximum temperature of the fluid is found optimum for the lowest *Re* as well as *Ri.*

- The influence of Prandtl number on streamlines and isotherms are remarkable for the different values of *Ri*. Escalating the Prandtl number increases the average Nusselt number at the heated surface and devalues the maximum temperature of the fluid.

Nomenclatures

D	outer diameter of the cylinder (m)
g	gravitational acceleration (ms^{-2})
k_f	thermal conductivity of fluid ($Wm^{-1}K^{-1}$)
k_s	thermal conductivity of solid ($Wm^{-1}K^{-1}$)
K	thermal conductivity ratio of the solid and fluid
L	length of the each side of the octagon (m)
Nu	Nusselt number
p	dimensional pressure (Nm^{-2})
P	non-dimensional pressure
Pr	Prandtl number
q	generated heat per unit volume (Wm^{-3})
Q	heat generating parameter
Re	Reynolds number
Ri	Richardson number
T	dimensional temperature (K)
u, v	velocity components (ms^{-1})
U, V	non-dimensional velocity components
x, y	Cartesian coordinates (m)
X, Y	non-dimensional Cartesian coordinates

Greek symbols

α	thermal diffusivity (m^2s^{-1})
β	thermal expansion coefficient (K^{-1})
υ	kinematic viscosity of the fluid (m^2s^{-1})
θ	non-dimensional temperature
ρ	density of the fluid (Kg m^{-3})

Subscripts

max	maximum
h	hot
i	inlet state
s	solid

References

1. V. V. Calmidi and R. L. Mahajan, Int. J. Heat and Fluid Flow **19**, 358 (1998). http://dx.doi.org/10.1016/S0142-727X(98)00002-2
2. Omri, S. B. Nasrallah, Num. Heat Transfer, Part A **36**, 615 (1999).
3. S. Singh, M. A. R. Sharif, Num. Heat Transfer, Part A **44**, 233 (2003).
4. O. Manca, S. Nardini, K. Khanafer, and K. Vafai, Num. Heat Transfer, Part A **43**, 259 (2003). http://dx.doi.org/10.1080/10407780307310
5. O. Manca, S. Nardini, and K. Vafai, Experi. Heat Transfer **19**, 53 (2006). http://dx.doi.org/10.1080/08916150500318380

6. S. Z. Shuja, B. S. Yilbas, M. O. Iqbal, Int. J. Num. Meth. Heat and Fluid Flow **10**, (8) 824 (2000). http://dx.doi.org/10.1108/09615530010359120
7. T. C. Hung and C. S. Fu, Numer. Heat Transfer, Part A **35**, 519 (1999).
8. M. Najam, A. Amahmid, M. Hasnaoui, and M. E. Alami, Int. J. Heat and Fluid Flow **24**, 726 (2003). http://dx.doi.org/10.1016/S0142-727X(03)00063-8
9. Y. L. Tsay, J. C. Cheng, T. S. Chang, Numer. Heat Transfer, Part A **43**, 827 (2003).
10. M. T. Bhoite, G. S. V. L. Narasimham, and M. V. K. Murthy, Int. J. Therm. Sci. **44**, 125 (2005). http://dx.doi.org/10.1016/j.ijthermalsci.2004.07.003
11. M. M. Rahman, S. Parvin, R. Saidur, and N. A. Rahim, Int. Commun. Heat and Mass Transfer **38**, 184 (2011). http://dx.doi.org/10.1016/j.icheatmasstransfer.2010.12.005
12. N. M. Brown, F. C. Lai, Int. Commun. Heat Mass Transfer **32** (8), 1000 (2005). http://dx.doi.org/10.1016/j.icheatmasstransfer.2004.10.029
13. G. Saha, S. Saha, M. N. Hasan, and M. Q. Islam, IJE Trans. A: Basics **23** (1), 1 (2010).
14. M. M. Rahman, M. A. Alim, M. A. H. Mamun, M. K. Chowdhury, and A. K. M. S. Islam, ARPN J. Eng. Appl. Sci. **2** (2), 25 (2007).
15. R. Nasrin, J. Sci. Res. **3** (3), 501 (2011). http://dx.doi.org/10.3329/jsr.v3i3.7433
16. R. Nasrin, J. Sci. Res. **4** (1), 39 (2012). http://dx.doi.org/10.3329/jsr.v4i1.8014
17. J. N. Reddy, An Introduction to Finite Element Analysis (McGraw-Hill, New York, 1993).
18. O. C. Zeinkiewicz, R. L. Taylor, and J. M. Too, Int. J. Numer. Meth. Engg. **3**, 275 (1971).
19. S. Roy and T. Basak, Int. J. Engg. Sci. **43**, 668 (2005). http://dx.doi.org/10.1016/j.ijengsci.2005.01.002